ALUMINUM CHLORINE BATTERY

BY JOSÉ GINER AND GERHARD L. HOLLECK

AUGUST 1969

Prepared under Contract No. NAS 12-688 by

TYCO LABORATORIES, INC.
WALTHAM, MASSACHUSETTS 02154

ELECTRONICS RESEARCH CENTER
NATIONAL AERONAUTICS AND SPACE ADMINISTRATION

Dr. Sol Gilman, CPE
Technical Monitor
NASA, Energy Conversion Branch
Electronics Research Center
575 Technology Square
Cambridge, Massachusetts 02139

Requests for copies of this report should be referred to:

NASA Scientific and Technical Information Facility
P. O. Box 33
College Park, Maryland 20740

NASA

ALUMINUM CHLORINE BATTERY

By José Giner and Gerhard L. Holleck

Fifth Quarterly Report
Covering Period
27 April 1969 — 26 August 1969

Prepared under Contract No. NAS 12-688 by

TYCO LABORATORIES, INC.
Waltham, Massachusetts 02154

Electronics Research Center
NATIONAL AERONAUTICS AND SPACE ADMINISTRATION

Table of Contents

List of Illustrations

ALUMINUM CHLORINE BATTERY

By José Giner and Gerhard L. Holleck

Tyco Laboratories, Inc.
Bear Hill
Waltham, Massachusetts 02154

SUMMARY

During the present reporting period, we continued our investigation of the behavior of the Al electrode in $AlCl_3$-KCl-NaCl melts. Experiments were conducted in quiescent electrolyte and at a rotating Al disk electrode. A special cell arrangement was used to allow microscopic, in situ observation of the Al electrode during polarization.

The results of these measurements confirmed our earlier findings that the observed passivation of the Al electrode is caused by formation of a solid salt layer at the electrode surface resulting from concentration changes upon anodic or cathodic current flow. The cathodic behavior is further complicated by dendrite growth which causes the electrode to expand into the melt.

It is evident that the values of the steady state current obtained are determined by diffusion processes and melt composition. Preliminary investigation of the $AlCl_3$-KCl-NaCl phase diagram by differential thermal analysis showed that the melting temperature increases very rapidly when the $AlCl_3$ content of the melt is increased from approximately 65 to 75 mol %.

INTRODUCTION

A molten salt system based on an Al anode and Cl_2-carbon cathode in an $AlCl_3$-alkali chloride melt as the electrolyte has been proposed by us. This system offers promise as a rechargeable, high energy density battery which can operate at a relatively low temperature. Recently, we reported our investigations showing both the potential and problems inherent to this system (Ref. 1). A procedure was developed to purify commercially available $AlCl_3$, thus enabling us to prepare clear and nearly colorless $AlCl_3$-KCl-NaCl melts.

Investigations of vitreous carbon electrodes showed that carbon is intrinsically active for chlorine reduction in $AlCl_3$-alkali chloride melts. A study of the compatibility of carbon electrodes with chlorine in $AlCl_3$ eutectics uncovered carbon samples which appear suitable for the construction of porous chlorine cathodes.

Passivation phenomena have been observed upon cathodic and anodic polarization of the aluminum electrode in $AlCl_3$-KCl-NaCl melts. It was established that they were not due to an electrochemical (potential-dependent) process, but were caused by formation of a solid salt layer at the electrode surface resulting from concentration changes upon anodic or cathodic current flow. The value of the steady-state current was determined by diffusion processes in the melt and the concentration change necessary to pass the liquidus curve of the phase diagram. The electrode behavior upon cathodic polarization was further complicated by dendrite growth, which caused the electrode to expand into the melt.

In the present reporting period, we continued the investigation of Al electrode behavior in $AlCl_3$-KCl-NaCl melts by employing various experimental methods.

THE Al ELECTRODE IN $AlCl_3$-KCl-NaCl MELTS

Al Electrode in Quiescent Molten Salt Electrolyte

To supplement our previous measurements (Ref. 1), we conducted polarization experiments at an Al wire electrode (0.26 cm^2) at 126 and 157 °C in an $AlCl_3$-KCl-NaCl melt (57.5-12.5-30 mol %). The salt mixture of this composition formed a clear melt at approximately 120 °C. This melt contains about the same KCl/NaCl ratio as the binary eutectic of $KAlCl_4$ and $NaAlCl_4$, in contrast to the melts previously employed which contained various amounts of $AlCl_3$ at the fixed KCl/NaCl ratio of the ternary eutectic. A melt composition similar to the one given above promises to be more favorable than the ternary eutectic, from a practical point of view, since it stays liquid over a wider concentration range at temperatures around 130 °C.

The electrochemical measurements consisted of slow cathodic and anodic potential sweeps, recording of current versus time curves at different preset cathodic and anodic potentials, and potential-time curves using constant current pulses.

Figs. 1 and 2 show two slow anodic and cathodic sweeps at 126 and 157 °C. The general shape of the current-voltage curves at the Al electrode was very similar to those found earlier in melts of different composition. The anodic region of the current-voltage curves was characterized by a limiting current which was dependent on temperature (it was about 35 mA/cm^2 at 120 °C and 100 mA/cm^2 at 157 °C). The anodic current maximum in Fig. 1 was very likely due to supersaturation of the melt close to the electrode. After the first crystals formed, the supersaturation ceased, resulting in a passivating salt layer at the electrode. This is responsible for the following current decreases. The same behavior appears in Fig. 3 in which the current is recorded as a function of time upon polarizing the electrode potentiostatically to +150 mV. The value for the anodic limiting current reflects the rate at which the passivating salt layer dissolves in the molten electrolyte.

Upon cathodic polarization, one finds a slight indication of a limiting current followed by a progressive current increase due to dendrite formation. Below 35 mA/cm^2 at 157 °C and 12 mA/cm^2 at 126 °C, there seems to be little dendrite growth, as indicated by the absence of a current increase with time (up to 10 min) at constant potential.

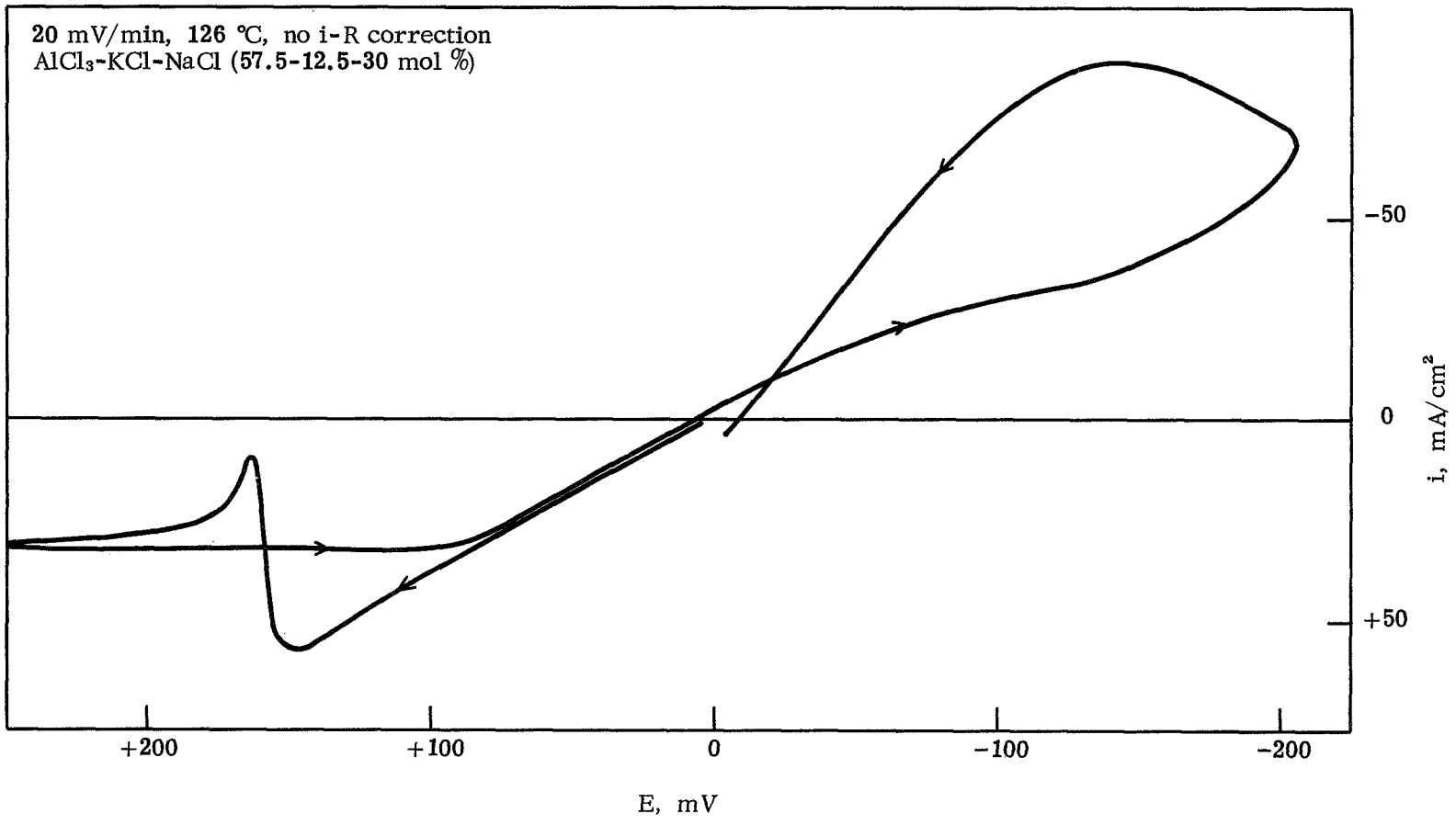

Fig. 1. Separate triangular anodic and cathodic potential scans at Al electrode

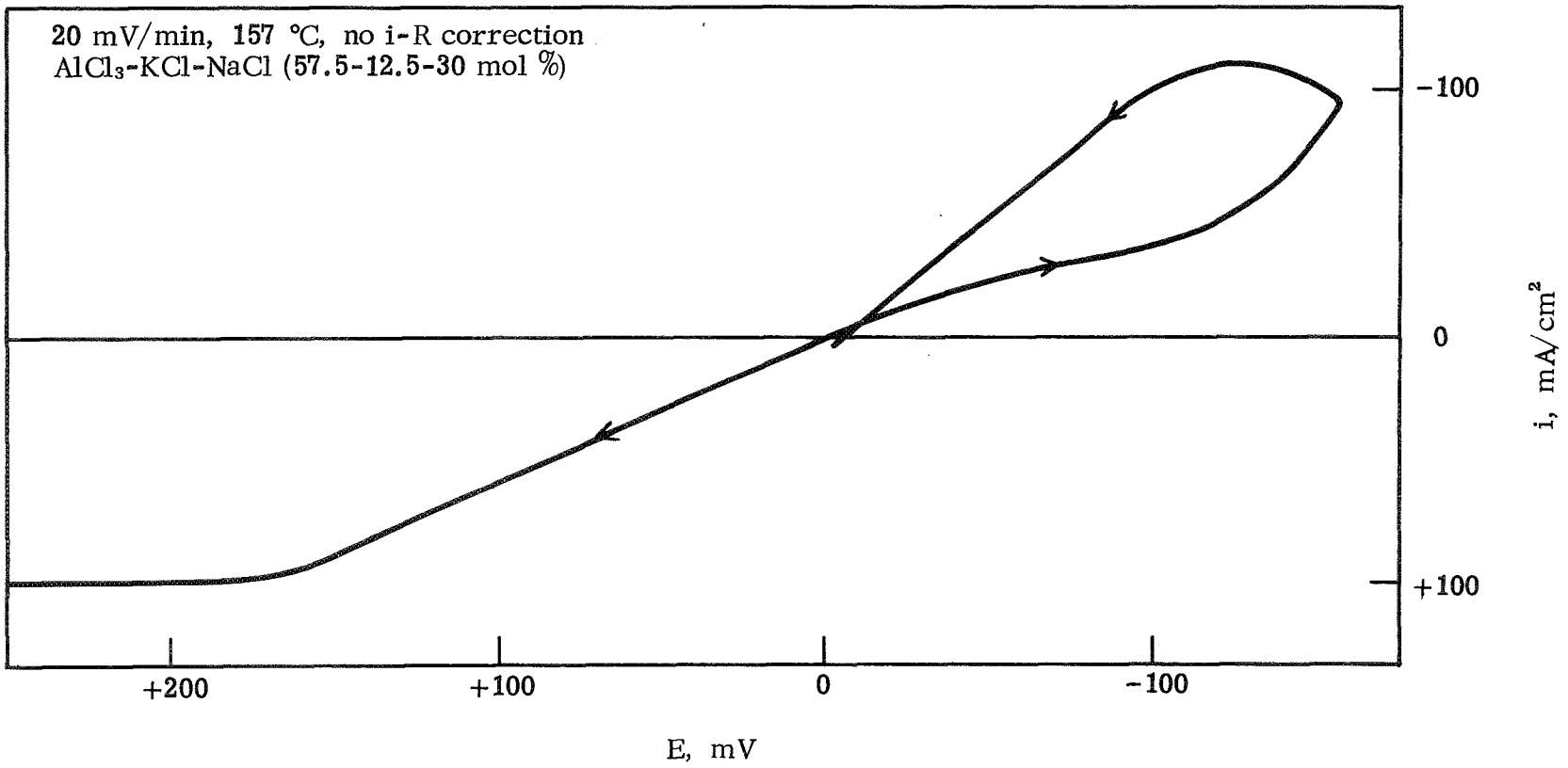

Fig. 2. Separate triangular anodic and cathodic potential scans at Al electrode

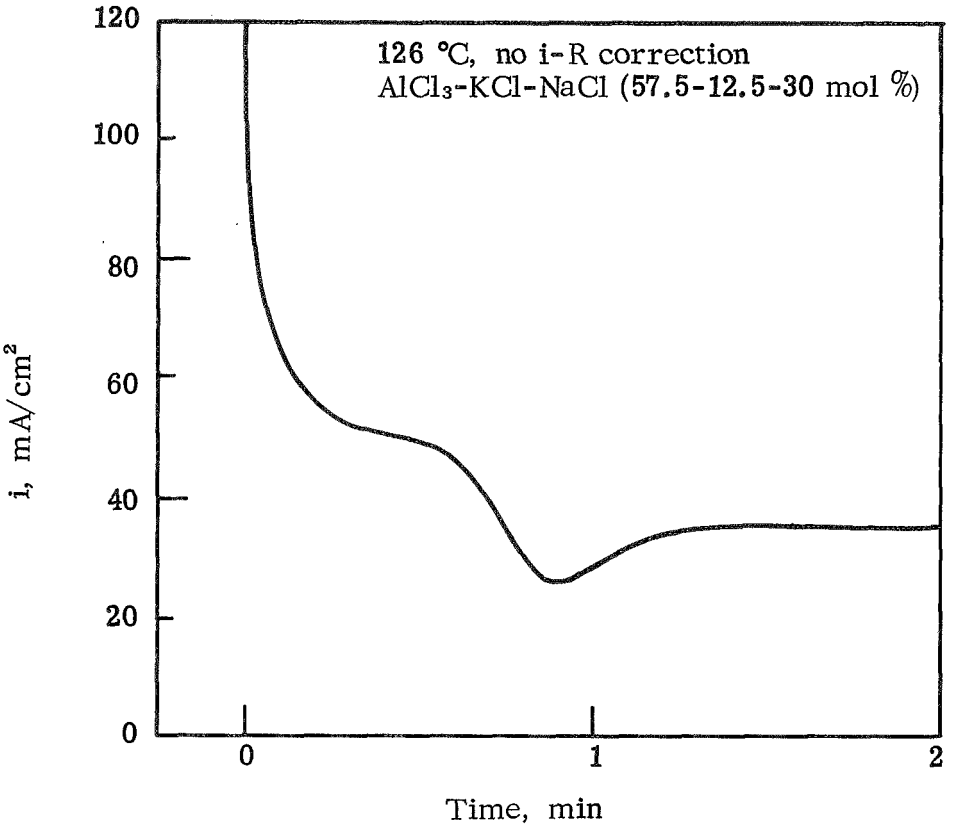

Fig. 3. Anodic current as function of time upon potentiostatic polarization of Al electrode to 150 mV versus Al reference

The results of these measurements confirm our earlier findings that the observed passivation is caused by the formation of a solid salt layer at the electrode surface resulting from concentration changes upon anodic or cathodic current flow. It is further evident that the values of the steady-state current obtained are determined by diffusion processes and melt composition, as discussed in detail in our previous report.

Table I summarizes some measured values for the i-R drop between the reference and working electrode as determined by galvanostatic pulse measurements. The corresponding resistances were found to be 2.0 ohms at 157 °C and 3.16 ohms at 126 °C. These values reflect the relative changes in the conductivity of the melt as a function of temperature. The electrolyte conductivity around the working electrode will, however, change considerably during steady-state current flow as a consequence of the occurring concentration changes.

TABLE I

GALVANOSTATIC PULSE MEASUREMENTS

Current, mA	Resistance, ohms	
	Anodic Pulse	Cathodic Pulse
	Temperature = 126 °C	
1.9	3.18	3.12
4.8	3.16	3.22
9.4	3.17	3.17
48.0	3.16	3.10
	Temperature = 157 °C	
1.9	2.06	2.04
4.8	1.92	2.11
9.4	1.90	2.03
48.0	1.86	1.86

The galvanostatic pulse measurements confirm our earlier findings that the activation overvoltage in the molten salt electrolyte is small.

In general, our measurements show that in the present system we are dealing with a very small activation polarization component, and a relatively large concentration polarization component. Thus, in order to measure the activation polarization accurately, it is necessary to employ pulses of high current density with short rise time. It is further necessary to compensate for the ohmic potential drop between working and reference electrodes in order to record the potential-time curves on a sufficiently sensitive oscilloscope scale. Such measurements are presently in progress.

Effect of Mass Transport in the Melt

A rotating disk apparatus has been constructed, and preliminary current-voltage curves have been obtained as a function of rotation speed.

The Al electrode consisted of a disk of 0.382 cm^2 geometric area press-fitted into thick-walled Teflon tubing. A Teflon balljoint was connected to the shaft by an O-ring press fitting and rotated in a corresponding glass socket joint. An Al counterelectrode (about 14 cm^2) served also as the reference electrode.

Polarization measurements conducted at 125 °C in an $AlCl_3$-KCl-NaCl melt, with 57.5-12.5-30 mol % of the respective components, demonstrate clearly the large influence of transport phenomena on the current-potential behavior of the Al electrode. For example, the measured anodic currents at a potential difference of 50 mV between working and counterelectrode increase from 23 mA/cm^2 at the stationary electrode to 56 mA/cm^2 at a rotation speed of 32 rps.

If the current, i, at a rotating disk electrode is diffusion controlled, the relation between i and the rotation speed should obey Levich's equation (Ref. 2):

$$i = 0.620\, nFD^{2/3}\, \upsilon^{-1/6}\, \omega^{1/2}\, \Delta C$$

where n = number of electrons transferred, F = Faraday constant, D = diffusion coefficient, υ = kinematic viscosity, $\omega = (2\pi r)^{1/2}$, where r = rotations per second, and ΔC = concentration gradient of active species. In the applicable range of this equation, a plot of i versus $\omega^{1/2}$ should give a straight line intersecting the origin, if all other parameters remain constant.

Table II and Fig. 4 show the change of the anodic limiting current as a function of $\omega^{1/2}$. A nearly linear relation between limiting current density and the square root of the angular velocity was observed. There is some deviation from linearity and some variation in the individual current densities, but these were expected. One must keep in mind that we are actually dealing with the dissolution of a passivating solid salt layer at the surface of the rotating electrode, which is in many respects quite different from the idealized conditions for which the above equation is strictly valid. Furthermore, at the high current densities observed, changes in the electrode itself cannot be avoided. For example, the lower current value at the high rotation speed is very likely due to the formation of a recess in the Al electrode caused by Al dissolution at high current density. Therefore, the aluminum disk surface does not remain flush with the outer Teflon sheathing.

TABLE II

ANODIC LIMITING CURRENT AS A FUNCTION OF ROTATION RATE AT 125 °C [$AlCl_3$-KCl-NaCl (57.5-12.5-30 MOL %)]

RPS	$\omega^{1/2}$	i, mA	mA/cm^2
0	—	7	18.2
3.7	4.82	41	106.5
8.5	7.31	75	194.8
14.1	9.41	100	259.7
23.3	12.10	128	332.5
43.8	16.59	144	374
0	—	7	18.2
3.75	4.85	44	114.3
9.5	7.73	85	220.8
19.2	10.98	107	277.9

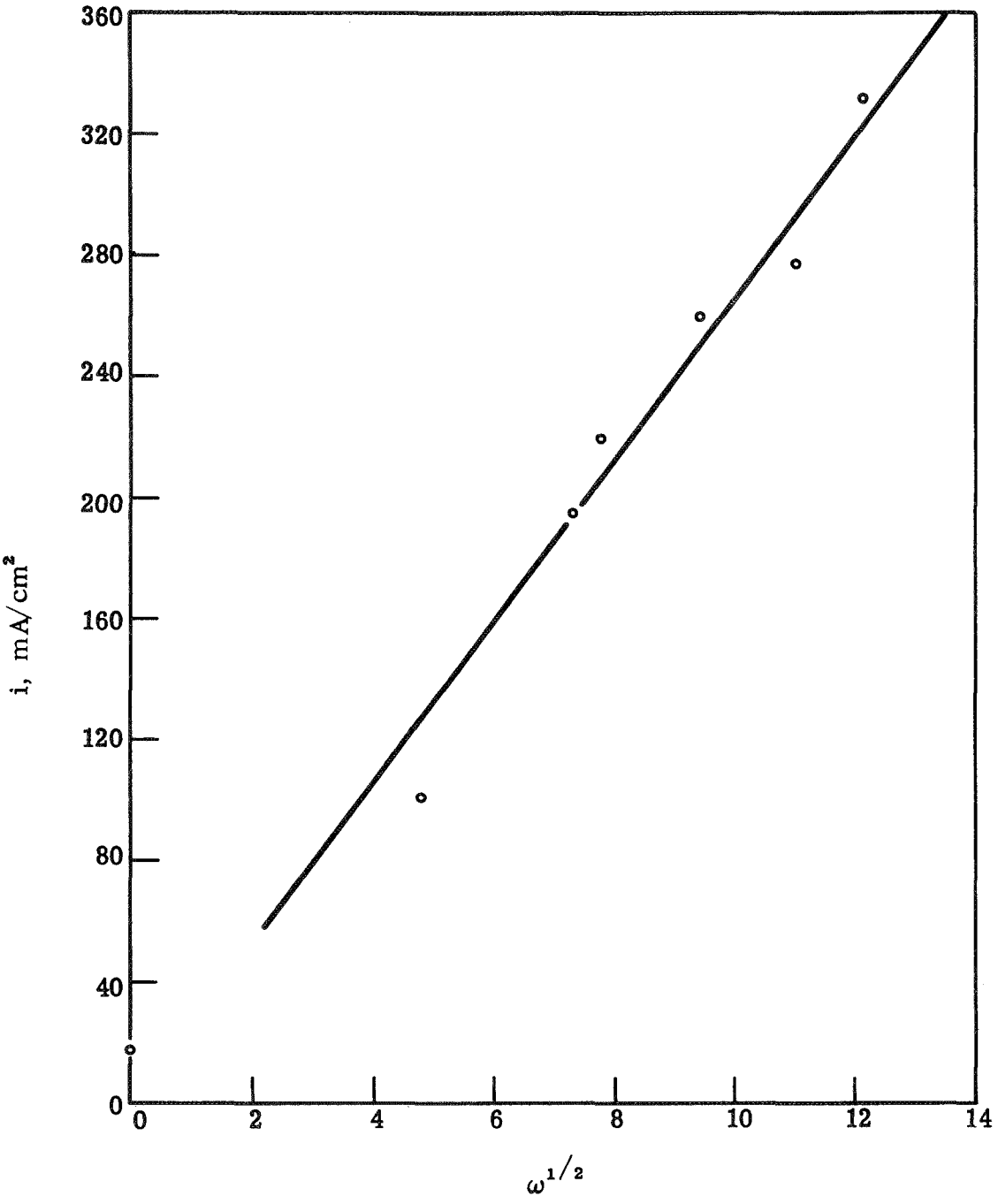

Fig. 4. Anodic limiting current as a function of rotation rate at Al disk in $AlCl_3$-KCl-NaCl (57.5-12.5-30 mol %) at 125 °C

These results show clearly the role of mass transport in removing reaction products from the electrode surface. They show further that high current densities can be obtained at Al electrodes at relatively low temperature, if the transport limitations can be overcome.

During the operation of the rotating disk electrode, some shortcomings of the arrangement became apparent. They are mainly related to the mechanical feed-through of the rotating shaft. We plan to use this experience to build a more reliable arrangement which can also be used to study the kinetics of the Cl_2 electrode on vitreous carbon electrodes.

Microscopic In Situ Observation of the Al Electrode During Polarization

Experimental. - The experimental cell consisted of a 100-ml, round-bottom, four-neck Pyrex flask with a flat Pyrex glass window at the bottom (the cell is shown in Fig. 5). The disk electrode was press-fitted into Teflon tubing and extended about 6 mm from the glass window. The counterelectrode consisted of several loops of Al wire. A rubber balloon was used as a flexible argon reservoir. All connections were made with standard taper Teflon connectors containing O-ring press fittings. For measurements, the cell was heated in a small oven with a hole (1.5 cm^2) in the bottom for microscopic observation. An exploded view of the basic setup with the Leitz metallograph is shown in Fig. 6.

Results. - The experiments were conducted in an $AlCl_3$-KCl-NaCl melt (57.5-12.5-30 mol %) at 133 °C. Figs. 7 through 10 show the electrode at different stages of polarization.

The electrode showed an etched surface appearing as dark and bright planes in partially polarized light. The formation of gas bubbles could also be observed. They appeared to form mainly on the aluminum surface, independent of polarization. Only at an anodically passivated electrode was a markedly decreased rate of bubble formation observed. The nature of this gassing is not clear at present. The most likely explanation seems to be a supersaturation of the melt with argon leading to the formation of small bubbles at the Al-melt interface, which then grow by incorporation of $AlCl_3$ vapor. Another possible source of gas formation could be the reaction of $AlCl_3$ with moisture leading to HCl.

Fig. 7 shows an example of the dendrites formed at the electrode during cathodic polarization. Below 50 mA/cm^2, there seemed to be little dendrite forma-

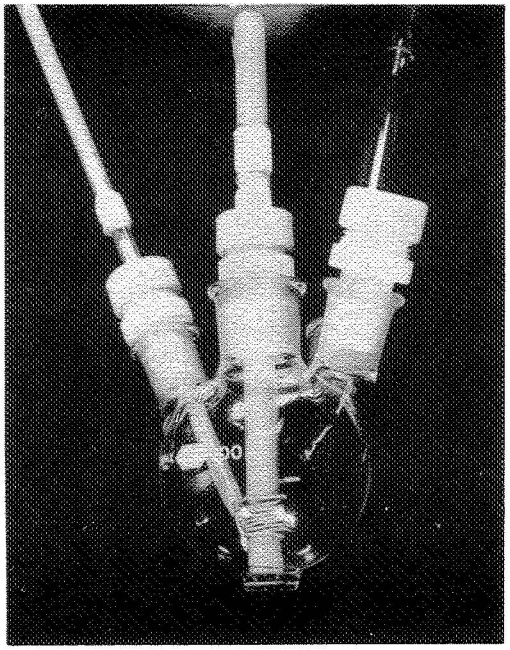

Fig. 5. Cell for in situ microscopic observation of a disk electrode

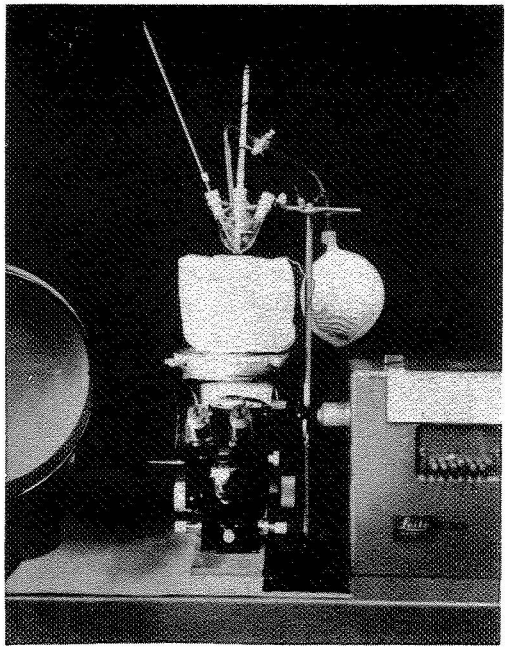

Fig. 6. Experimental setup for in situ microscopic observation (exploded view of Al electrode)

Fig. 7. Dendrites at Al electrode (25X) in $AlCl_3$-KCl-NaCl (57.5-12.5-30 mol %) at 133 °C

Fig. 8. Al electrode covered by passivating salt layer (25X) in $AlCl_3$-KCl-NaCl (57.5-12.5-30 mol %) at 133 °C

Fig. 9. View through gas bubble on anodically polarized Al electrode (25X) in $AlCl_3$-KCl-NaCl (57.5-12.5-30 mol %) at 133 °C

Fig. 10. Area of anodically polarized Al electrode after gas bubble left (25X) [$AlCl_3$-KCl-NaCl-(57.5-12.5-30 mol %) at 133 °C]

tion. At higher current densities (up to 263 mA/cm^2), heavy dendrite formation can be observed. Upon reversing the current, the dendrites partially dissolve anodically and separate from the electrode.

A sufficiently high anodic current led to passivation of the electrode due to salt formation. Such a passive electrode is shown in Fig. 8. Fig. 9 shows an area of the Al electrode through a large gas bubble which shields the surface from the anodic current. After the bubble left the electrode, a bright reflecting area appeared (Fig. 10), which then turned into the passivated state (Fig. 8).

It was quite interesting to watch the growth of a gas bubble at the passivated electrode. One could observe strong motion at the gas-electrode-melt interface accompanied by transport of solid salt along the gas-liquid interface to the top of the bubble. This salt seemed to disappear by partial evaporation into the bubble and by dissolution in the melt. Thus, the electrode area underneath the bubble was not covered by a passivating layer, but appeared equal to an etched electrode in the gas phase. Occasionally, one could see small circular residues from an incompletely decomposed passivating layer (see Fig. 9).

The behavior of the Al electrode, seen here by direct microscopic observation, agrees perfectly with our earlier findings, and further confirms our concept of the processes occurring at the Al electrode in the molten salt electrolyte.

$AlCl_3$-KCl-NaCl PHASE DIAGRAM

The binary phase diagrams of $AlCl_3$-KCl, $AlCl_3$-NaCl, and $NaAlCl_4$-$KAlCl_4$, as well as the ternary phase diagram up to an $AlCl_3$ content of 50 mol %, have been investigated by several authors and were discussed previously. However, there is little known about the ternary phase diagram in the $AlCl_3$-rich region. Since this region represents the low melting part of the $AlCl_3$-KCl-NaCl phase diagram, it deserves central attention with regard to a molten electrolyte for an Al/Cl_2 battery. We therefore started an investigation of the $AlCl_3$-rich part of the ternary phase diagram using differential thermal analysis.

The $AlCl_3$-KCl-NaCl samples were prepared in the following way: KCl and NaCl, in the ratio KCl/NaCl = 0.7, were ground and carefully mixed. The final compositions were made up using this mixture and pure $AlCl_3$. The salt mixture was put into a quartz ampoule (the empty space was reduced by inserting another ampoule with smaller diameter), then evacuated and sealed. The bottoms of the quartz ampoules were ground to reduce wall thickness and obtain a better thermal contact between the sample and the thermocouple. For the measurements, a commercial differential thermal analyzer (model 16-A, T&T Control Co. Inc., Media, Pennsylvania) was used, and the difference in temperature between the sample and an Al reference versus the sample temperature was recorded on an x-y recorder. Two examples of such recordings are shown in Fig. 11. The cooling curves show large supercooling effects and were not used for evaluation. The results obtained from the heating curves are summarized in Fig. 12.

It is not possible at present to interpret these results with any certainty. The values obtained for the ternary eutectic and for the primary crystallization at $AlCl_3$ concentrations above 75 mol % seem to be too high. These preliminary measurements show, however, that sample preparation presents the largest problem. Some of the other contributing factors are the relatively small thermal effects of the melt, poor thermal contact between the sample and the thermocouple, and problems arising from sublimation of $AlCl_3$ due to temperature gradients along the sample. Thus, it is apparent that much more attention will have to be given to sample preparation in order to obtain more accurate results.

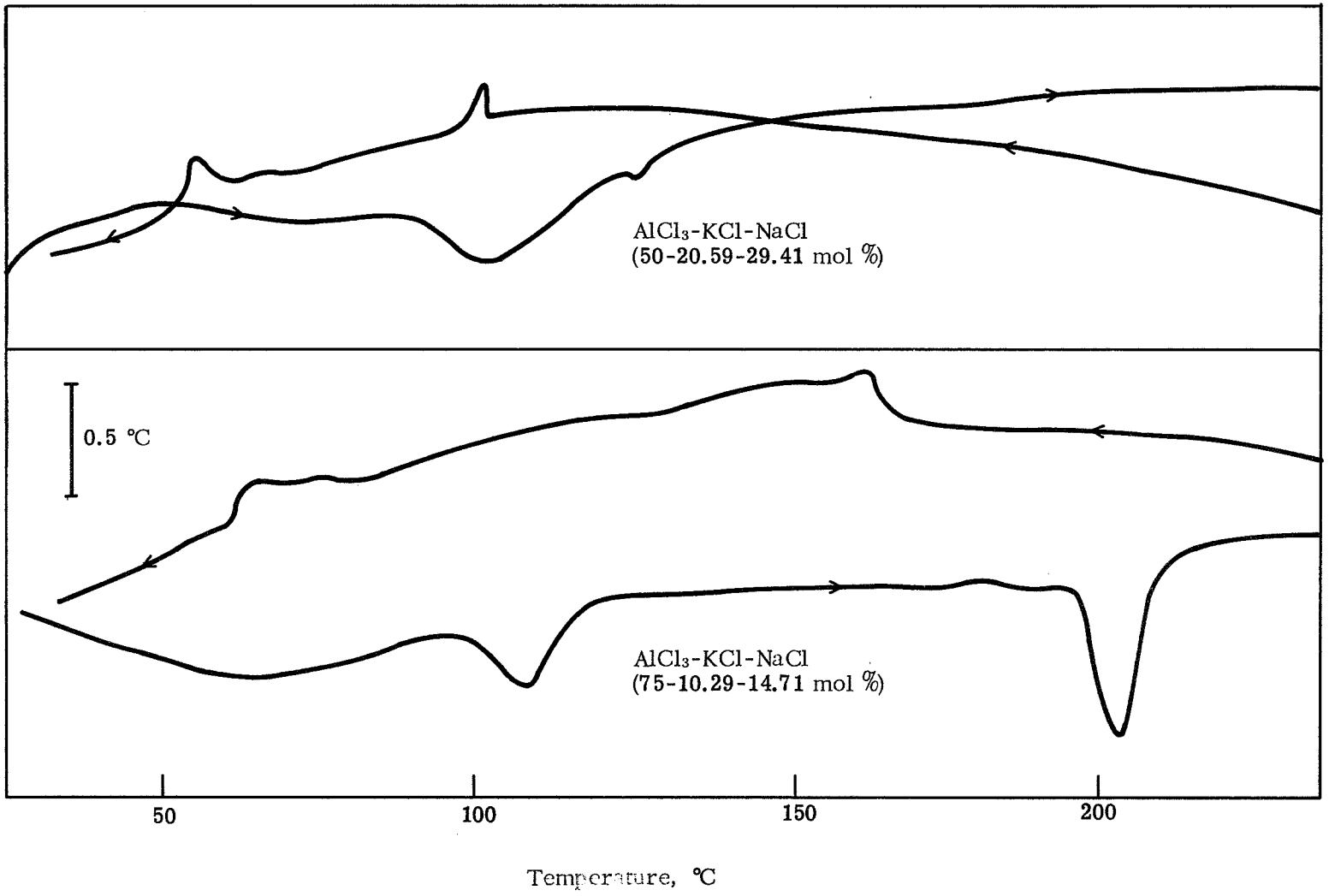

Fig. 11. Differential thermal analysis curves (Al_2O_3 reference; heating rate = 4°/min)

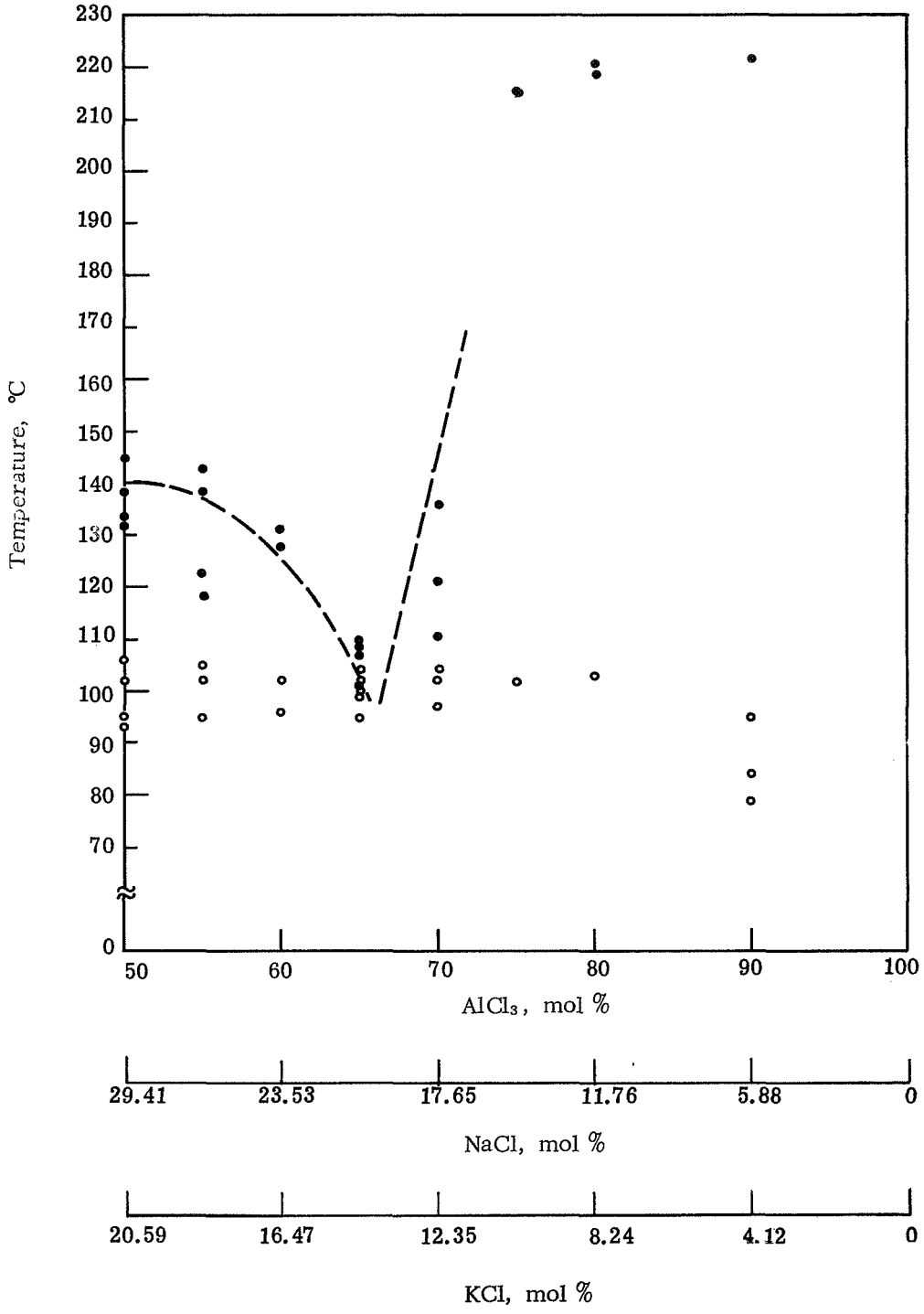

Fig. 12. Cut through $AlCl_3$-rich part of $AlCl_3$-KCl-NaCl phase diagram (preliminary measurements)

REFERENCES

1. Giner, J. and Holleck, G.: Interim Annual Report on Contract No. NAS 12-688, September 1969.

2. Levich, V. G.: "Physicochemical Hydrodynamics," Prentice-Hall, Inc., 1962.